Int J Adv Manuf Technol (2018) 94:327–339
DOI 10.1007/s00170-017-0889-6

ORIGINAL ARTICLE

Quality assessment of resistance spot welding process based on dynamic resistance signal and random forest based

Bobin Xing[1,2] · **Yi Xiao**[2] · **Qing H. Qin**[1,2] · **Hongzhi Cui**[1]

Received: 17 May 2017 / Accepted: 24 July 2017 / Published online: 10 August 2017

Abstract A scheme for online quality monitoring of resistance spot welding (RSW) process is proposed to effectively determine the rate of spot weld quality. In this work, the random forest (RF) classification featuring with dynamic resistance (DR) signals which were collected and processed in the production environment was carried out. The obtained results demonstrated that the constructed RF model based on DR profile features adequately distinguished high-quality welds from the other unacceptable welds such as inadequate sized welds and expulsions. Variable importance evaluation of RF was implemented against the input features. It showed that two DR slopes for nugget nucleation and growth (v_2, v_3) and dynamic resistance (R_γ) in the final half cycle play the most significant roles in achieving more accurate results of classification, while absolute gradient ∇_{max} is useful in detecting minor expulsion from pull-out failure. In addition, shunting effect in consecutive welds was tentatively investigated via the DR curves, accounting for noticeable declines in the stage I of DR. The results revealed that shunted welds beyond minimum weld spacing do not significantly undermine the accuracy of classification. The implementation of RF based on the combination of welding parameters and DR features improves the accuracy of classification (98.8%) with *ntree* = 1000 and *mtry* = 4, as weld current significantly distinguished situations where DR features solely achieve accuracy (93.6%). The incorporation of the RF technique into online monitoring system attains a satisfying RSW quality classification accuracy and reduces the workload on destructive tests.

Keywords Resistance spot welding · Random forest · Dynamic resistance · Quality control · Variable importance evaluation

1 Introduction

Resistance spot welding (RSW) is a popular joining technology for metal sheet assembly. It has been extensively used in many industrial fields, such as the automobile, aircraft manufacturing, owing to its ease of operation and wide applicability in automation. Efficiently monitoring the spot weld quality is desired. In fact, how to achieve high efficiency is challenging to researchers and engineers in this area. Unsatisfactory welds could be delivered in the production line under improper welding parameters. For instance, inadequately sized weld nugget (cold weld) with insufficient deformation-bearing capacity could lead to catastrophic structural failure. On the other hand, expulsion, described as the expelled molten metals either at the faying surface or workpiece/electrode surface, undermines the joint strength due to substantial deficiency of nugget volume and thus reduces lifespan of electrodes due to ultrahigh temperature along electrode tip surface [1]. Therefore, it is utterly important to sustain weld quality consistent throughout the industrial production.

A number of destructive and non-destructive approaches have been undertaken for monitoring the welding quality. Destructive inspections, being performed on one sample basis off the production line, show appealing reliability in

✉ Qing H. Qin
Qinghua.Qin@anu.edu.au

1 Guangdong Provincial Key Laboratory of Durability for Marine Civil Engineering, Shenzhen University, Shenzhen 518060, China

2 Research School of Engineering, Australian National University, Acton, ACT 2601, Australia

Table 1 Research comparison on characterizing the process signals of RSW and constructed online monitoring system

Method	Data source	Base materials	Achievements	Drawbacks	Typical studies
Non-linear regression	ED	Mild Steel	Establishment of nonlinear relation between ED features and tensile shear strength	Expulsion ignored in the study	[10]
Random forest	UO	Mild Steel	Weld quality classifier based on UO signal, variable importance identified via RF approach, strong resistance to overfitting, and better classification accuracy over ANN and regression.	Off-line signal, UO, does not provide much development history of nugget as DR does	[9]
Artificial neural network	DR and weld parameters	Titanium Alloy	Satisfying prediction of weld quality based on principal components from DR signals and weld parameters	User fails to interpret ANN mechanism, and principal components derived from DR does not have much physical meaning	[11]
Chernoff face analysis	ED	Mild Steel	Effectively distinguish normal welds from expulsion and welds under abnormal conditions based on facial impression	Further processing on the facial impression to weld quality classifier relies on human operator judgment.	[12]
Random forest	DR and weld parameters	Mild Steel	On-line parameter DR and weld parameters are incorporated into RF to investigate individual and continuous welds. Shunting effect with minimum welding distance is considered.	The shunting effect on DR with small welding spacing is not studied.	Present Work

ED electrode displacement, *UO* ultrasonic oscillogram, *DR* dynamic resistance

distinguishing unsatisfactory welds from welds with high quality. However, the factors including the cost of implementation, the usage of material, and low productivity prevent them from being extensively employed in the plant environment. In contrast, non-destructive methods have utilized a number of process signatures to evaluate weld quality. For this purpose, off-line signals, ultrasonic, and on-line signals, mechanical and electrical have been sampled and processed. Since the components of these signals vary with respect to the nucleation and development of nuggets, they can be used to identify cold welds and expulsions from the acceptable welds.

Ultrasonic waveform, a kind of off-line signal, is employed for determining the final nugget diameter. It is found that the nugget diameter and relatively height of echoes and sequence of echoes are strongly closely related, though little information of nugget development history is provided [2]. To provide a good insight on the history of nugget development, mechanical signals such as electrode displacement are captured. Wang et al. demonstrated distinct signatures of expulsion or cold welds from good welds, owing to the thermal expansion associated with nugget growth [3]. However, he indicated that the constraints related to the cost of achieving high precision of displacement sensor make electrode displacement sampling only be favorable in laboratory environment, rather than plant environment. Consequently, a more affordable electrical signal, dynamic resistance (DR), is then proposed. Gedeon et al. highlighted that the ease of installation and process and the low cost in measurement allow this signature to be widely adopted in the production environment [4]. With the simultaneous collection of voltage and current signals during the welding phase, the DR curves can be derived from these signals at different stages which involve pronounced physical phenomena. The curves can differentiate weld qualities based on the appearance of the profile. The relative positions of the DR curves, varied by welding current and welding force, indicate whether the adequate nugget is formed [5]. Moreover, Fan et al. demonstrated the application of DR

Table 2 Chemical composition of CA2S-E (wt%)

Material	C	Si	S	P	Mn	Al
CA2S-E	0.04–0.07	0.005–0.01	0.008–0.02	0.005–0.02	0.18–0.25	0.03–0.05

Table 3 Mechanical properties of CA2S-E

	Ultimate strength (MPa)	Yield strength (MPa)	Elongation (%)
CA2S-E	160–250	270–340	34–46

curves in expulsion detection under various circumstances [6]. The sudden decline in DR curves, associated with ejection of molten metal, could indicate the presence of expulsion.

To improve the accuracy of weld quality monitoring, researchers have utilized various methods to characterize the process signals of RSW and construct monitoring system, as summarized in Breiman who proposed a pattern recognition technique, random forest (RF), as a mathematical model for classification [7]. The advantages of applying RF over current quality monitoring methods lie in the better interpretability of the algorithm and its capability of sorting out thousands of features and dealing with missing values. Variable importance evaluation provided by RF allows users to identify the importance of variables and possibly reduce the dimension of data. Also, current methods, such as artificial neural network (ANN) and non-linear regression, are prone to overfitting when the training set is improperly evaluated, while the RF exhibits the appealing overfitting resistance with increased number of trees [7]. So far, efficiently applying RF on monitoring RSW weld quality has rarely been demonstrated. We only found two ultrasonic signal orientated studies in laboratory environment. Martín et al. incorporated ultrasonic oscillograms into an RF classifier, in which four levels of the weld, such as good weld, no weld, undersized weld, and stick weld, were considered as the classes for RF classification [8]. Moreover, Pereda et al. compared a series of ultrasonic waveform-based classification methods including RF for the quality assessment of RSW. The classification results and receiver operating characteristic (ROC) curve showed that RF technique outperformed a number of popular classification methods such as ANN and logistic regression [9].

Table 1. Some challenges and issues remain in these methods. For instance, shunting effect is inevitable in the production line. Shunting current in RSW could deliver an apparent decrease in nugget diameter in consecutive welds on the same sheet, due to declined welding current [13]. The phenomenon can be expressed by the decline of DR values due to the parallel circuit of welding path and shunting path. However, existing studies on quality classifier did not cover this phenomenon in their constructed system. The inclusion of multiple welds on the same sheet is necessary for construct online monitoring systems in plant environment.

Table 4 Welding schedule used in this study

Weld current	Weld time	Electrode force	Hold time
8.0 kA	0.16 s	1700 N	0.2 s
8.8 kA	0.20 s	2000 N	
9.6 kA	0.24 s	2300 N	
10 kA		2700 N	
10.4 kA			
10.8 kA			
11.2 kA			

Breiman proposed a pattern recognition technique, RF, as a mathematical model for classification [7]. The advantages of applying RF over current quality monitoring methods lie in the better interpretability of the algorithm and its capability of sorting out thousands of features and dealing with missing values. Variable importance evaluation provided by RF allows users to identify the importance of variables and possibly reduce the dimension of data. Also, current methods, such as ANN and non-linear regression, are prone to overfitting when the training set is improperly evaluated, while the RF exhibits the appealing overfitting resistance with increased number of trees [7]. So far, efficiently applying RF on monitoring RSW weld quality has rarely been demonstrated. We only found two ultrasonic signal orientated studies in laboratory environment. Martín et al. incorporated ultrasonic oscillograms into an RF classifier, in which four levels of the weld, such as good weld, no weld, undersized weld, and stick weld, were considered as the classes for RF classification [8]. Moreover, Pereda et al. compared a series of ultrasonic waveform based classification methods including RF for the quality assessment of RSW. The classification results and receiver operating characteristic (ROC) curve showed that RF technique outperformed a number of popular classification methods such as ANN and logistic regression [9].

To advance the technique of monitoring weld quality of RSW from the laboratory to the plant environment, we propose the DR, a more reliable and affordable dynamic signature, over ultrasonic signal for monitoring weld quality of RSW. In this work, an experimental study of a RF-based classifier using DR signals of mild steel is presented. The welds made for RF construction were divided into test samples and consecutive welds, similar to the weld sequence in the production environment. We identified here how DR profile shunted welds varies from the normal welds when weld spacing is acceptable. Profile quantities with physical meanings were used for RF construction, whose importance to classification accuracy is further evaluated and ranked. Moreover, in this study, additional DR gradient and weld parameters were included to improve the accuracy of classification.

2 Experimental procedure and methodology

2.1 Material and equipment

The material used in the experiments was 1 mm cold rolled mild steel (CA2S-E), whose chemical composition and mechanical properties are manifested in Tables 2 and 3,

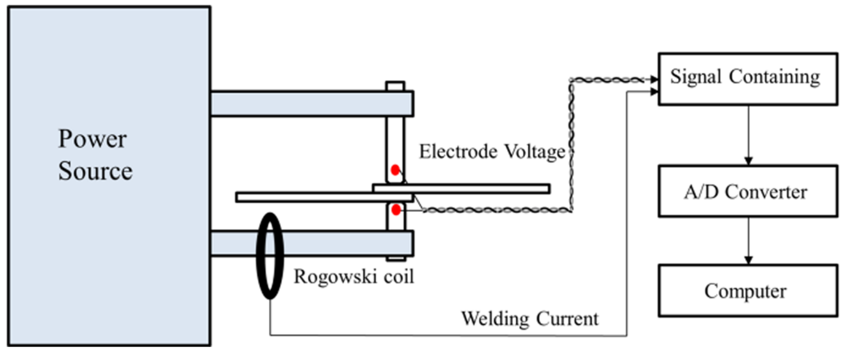

Fig. 1 Experimental set-up

respectively. The base materials were spot welded with a single-phase alternating current (AC) pedestal welder (50 Hz), along with water cooled truncated cone CuCrZr electrodes with 6-mm tip face diameter.

2.2 RSW process parameters and experimental set-up

There are four key parameters in a weld schedule, namely weld current (*WC*), weld time (*WT*), electrode force (*EF*), and hold time (*HT*). The first three parameters make contributions to the heat input in RSW, while the parameter of hold time accounts for the cooling rate of the weld nugget. This study utilizes DR curve on monitoring weld quality. Hold time does not differentiate DR. Thus, control variables in this study were selected as weld current, weld time, and electrode force only. Detailed welding parameters are shown in Table 4. To resemble the destructive test frequency in plant environment, two types of welds were made, namely destructive weld and continuous weld. In total, seven welds were made. Three destructive samples were selected and stretched until failure at every welding schedule. The other four continuous welds were made consecutively on the steel-steel workpieces with a weld spacing of 20 mm, in which shunting effect does not substantially affect the nugget size of bare mild steel [13]. The weld schedule began with weak parameters (small weld current and short weld time), while the electrode force was initially fixed at 1700 N. When expulsion was identified, the upcoming experiment under current welding schedule was terminated. The electrode force then increased to next level and weld current and weld time applied weak parameters again. Hence, not all combinations in Table 4 were carried out. In total, 368 welds were made, which were later used to construct RF models.

The layout of the experiment is shown in Fig. 1. The weld current was measured by the Rogowski coil placed at the lower arm of the welder, and the electrical voltage was derived from the voltage difference between two electrodes. To minimize the inductive noise caused by the AC waveform, the leads connecting two electrodes were twisted. The sampling rate was fixed at 10 kHz. An array of digitized data of voltage and current was acquired and processed to yield associated DR. In this work, we represent DR as the root-mean-square resistance per half cycle calculated via the following:

$$R_{RMS} = \frac{U_{RMS}}{I_{RMS}} \tag{1}$$

This approach substantially preserves the key signatures of DR.

2.3 Tensile shear test

The tensile shear test is a measurement of the quality of resistance welded joint. A joint is subjected to a pair of parallel forces until destruction. The tested specimens were prepared to a size of 100 mm × 25 mm, and the overlapped area was 25 mm × 25 mm as shown in Fig.

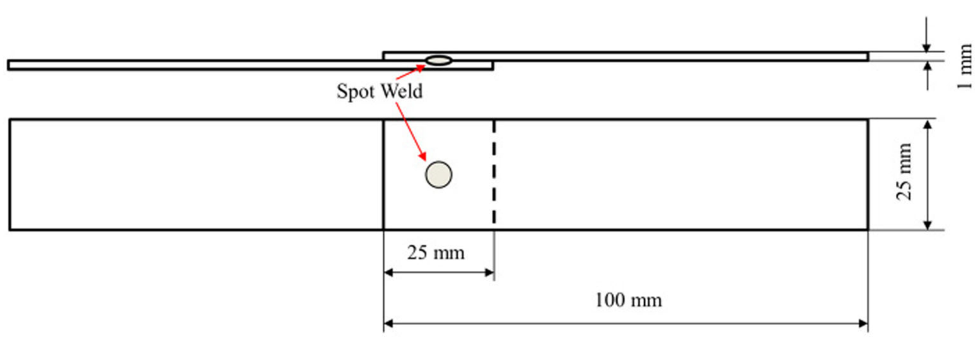

Fig. 2 Specimen dimension for tensile shear test

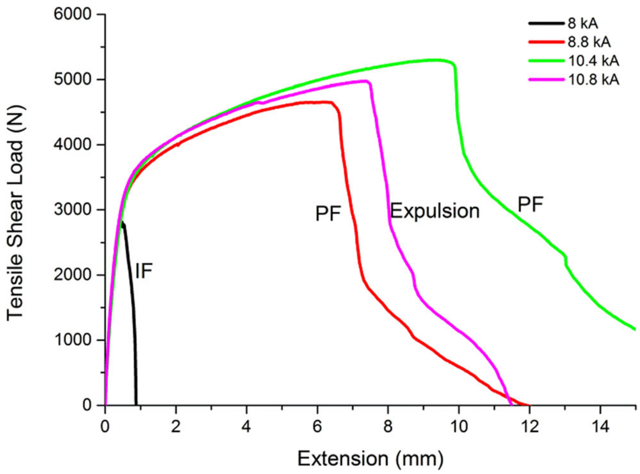

Fig. 3 Extension-load curves of different weld qualities

2 [14]. A tensile shear test was carried out under a crosshead velocity of 5 mm/min at room temperature. The peak value before the failure in the extension-force curve is recorded as the tensile shear load. The RSW quality is strongly function-related to failure mode and peak strength. Interfacial failure (IF) and pull-out failure (PF) are the two predominant failure modes in tensile shear test in RSW. Long et al. revealed that weld failure mode is determined by the competition between a tensile resistance force and a shear resistance force of the nugget [15]. When the maximum shear resistance force supplied via the interface of the weld nugget outweighs the maximum tensile resistance force supplied via the tensile cylindrical regions, the failure mode would be button pull-out; otherwise, it fails as an interfacial shear mode.

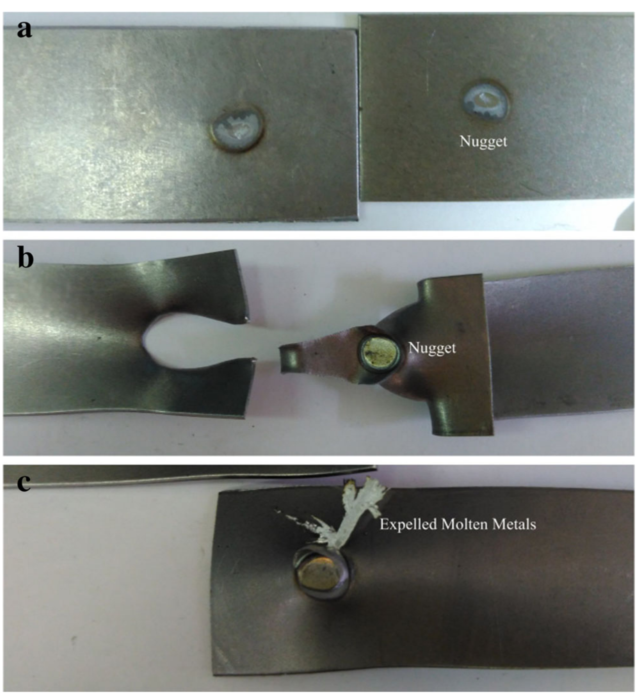

Fig. 4 Three types of RSW joints at failure. **a** Cold weld. **b** Good weld. **c** Expulsion

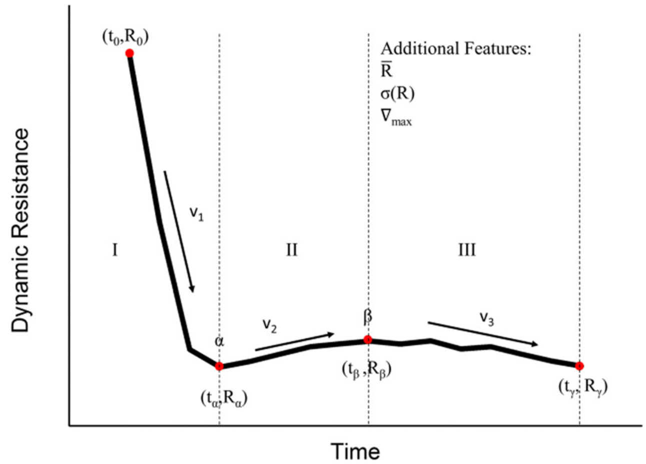

Fig. 5 Schematic diagram of extracted features of representative dynamic resistance curve

2.4 Random forest

In this study, an RF classifier was implemented, using the "random forest" R package [16]. RF method adopts an ensemble of independent decision trees $h_i\{\boldsymbol{X}\}$ ($i = 1,2\ldots$k). The classification result of the RF is an unweighted majority based on the voting of each independent tree, which is considered as a weak learner. Each tree is planted under independent random vector Θ of the identical distribution. Bootstrapping method creates *ntree* sample sets constituting of about $\frac{2}{3}$ of the original data set, in which *ntree* indicates the total number of trees. By performing bootstrapping method, there are approximately one-thirds of original data being unselected for each tree, referring to out-of-bag (*OOB*) data.

For every node in a k^{th} tree $h_i\{\boldsymbol{X}\}$ ($i = 1,2\ldots$k), *mtry* features are selected out of the total M feature of the input data. The value of *mtry* should be much less than M; otherwise, the correlation among trees strengthens. A large value of *mtry* adversely influences the accuracy and reliability of the RF classifier. The *mtry* features are employed to determine the optimum split variables and the best split point. This recursive step continues until a maximal tree is created, suggestive of the optimum split parameter for the current node is identical to that of the parent node. No pruning is carried out for every tree. These actions allow a low bias among the ensemble of decision trees. Likewise, randomization needs to be assured for an RF model. It is accomplished by a series of operations, including bootstrapping, a random *mtry* selection from each node, and optimization of the value of *mtry*. The low bias and low correlation guarantee reliability of the RF model. The

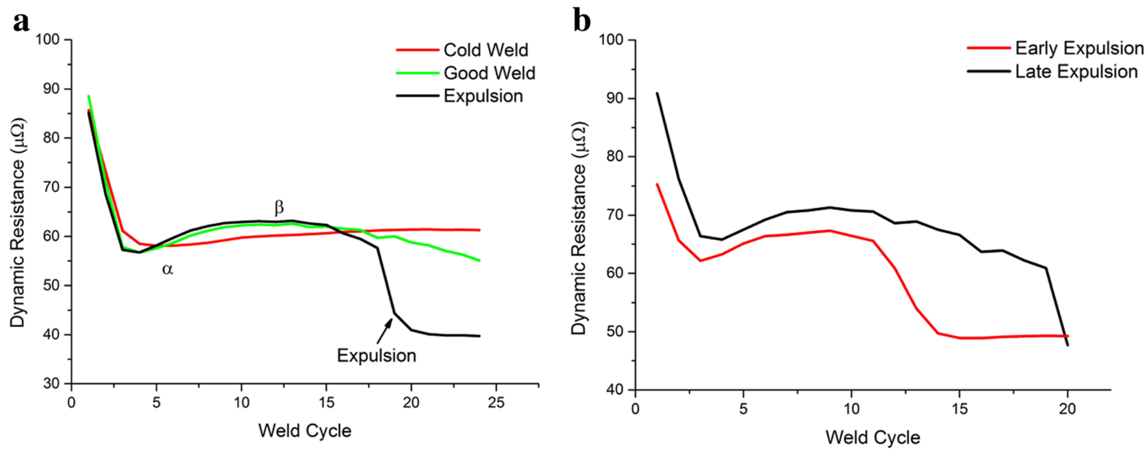

Fig. 6 **a** Representative dynamic resistance curves for three levels of joints at 12 weld cycles. **b** Representative dynamic resistance curves of early expulsion and late expulsion at 10 weld cycles

decisions of the parameters *ntree* and *mtry* tend to substantially impact on the accuracy of the classifier. A discussion on sensitivity to *ntree* and *mtry* was performed. Original data were divided into a training set (75%) and test set (25%). The RF models were constructed based on the training set, making the test set independent from the RF models. Ten-fold cross validation was conducted on training data to examine the overfitting.

3 Results

3.1 Class selection for RSW weld quality classification

Figure 3 demonstrates averaged load-extension curves of the tested specimens using different welding currents. It is straightforward to distinguish the interfacial failure and expulsion from the pull-out failure. The IF specimen does not exhibit an appealing tensile shear load bearing capacity prior to the failure, while the specimen with expulsion presents a downward trend in tensile-shear load and failure energy, though a greater heat input is applied. Specimens with PF mode attain a good combination of strength and ductility; thus, they were viewed as good welds. Furthermore, Fig. 4 displays three types of RSW weld failures after the tensile-shear test. Figure 4a shows the couplers rupture in the interfacial shear mode, suggestion of a cold weld formed during welding. In Fig. 4b, the specimen fails in PF mode. The weld nugget is preserved after the test. The failure takes place from the heated affected zone (HAZ) region, indicating that the HAZ is prone to deformation for a good weld. In Fig. 4c, we can observe the expelled molten metals on the faying surface. Deficiency of weld nugget occurs as the result of expulsion, and the mechanical performance is deteriorated as well. Based on the extension-load curve, the failure mode, and observation on expulsion, three levels of weld qualities were thus utilized as the classification response in the RF model, with regard to cold weld, good weld, and expulsion.

3.2 Characteristics of dynamic resistance signature on RSW

A group of current and voltage signatures were collected and processed for determining the DR signature. As

Table 5 Inter-variable correlation matrix

Variables	R_α	R_β	R_γ	v_1	v_2	v_3	R	σ	∇_{max}
R_α	1.00	0.95	0.48	0.18	0.23	− 0.33	0.89	0.23	− 0.26
R_β	0.95	1.00	0.58	0.11	0.40	− 0.28	0.94	0.16	− 0.19
R_γ	0.48	0.58	1.00	0.31	− 0.06	0.55	0.77	− 0.51	0.59
v_1	0.18	0.11	0.31	1.00	− 0.42	0.33	0.16	− 0.24	0.22
v_2	0.23	0.40	− 0.06	− 0.42	1.00	− 0.48	0.26	0.24	− 0.33
v_3	− 0.33	− 0.28	0.55	0.33	− 0.48	1.00	− 0.04	− 0.68	0.89
R	0.89	0.94	0.77	0.16	0.26	− 0.04	1.00	− 0.12	0.08
σ	0.23	0.16	− 0.51	− 0.24	0.24	− 0.68	− 0.12	1.00	− 0.83
∇_{max}	− 0.26	− 0.19	0.59	0.22	− 0.33	0.89	0.08	− 0.83	1.00

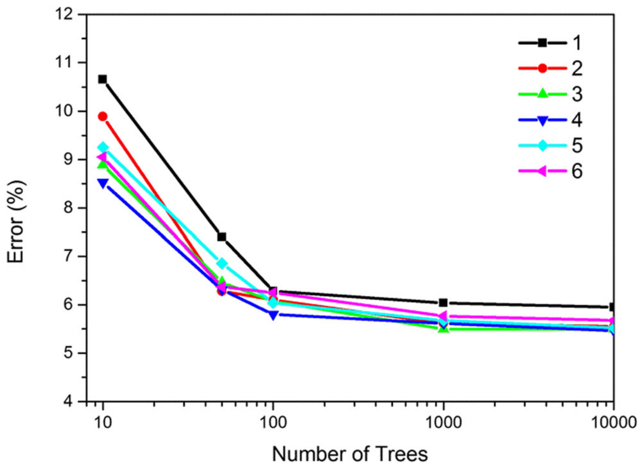

Fig. 7 Summary of influence of *ntree* and *mtry* on *OOB* misclassification error (%)

mentioned, root-mean-square DR was used to represent the dynamic signature. A higher resolution of DR signature could be evaluated by deriving the equation with an estimated value of L:

$$\frac{dI}{dt}L + IR = U \tag{2}$$

where L is the inductance of circuit, I is the current, R is the dynamic resistance, and U is the voltage. However, the nature of different weld time determines the different length of DR curves, making directly importing DR signature into RF classifier less favorable. Instead, we preferred to distract a number of characteristics to describe each DR plot. From the typical DR curve of mild steel in Fig. 5, we can see that the DR firstly declines until the trough α, and it again climbs to reach the β peak. After this extreme point, DR experiences a descending trend to the terminal point of the DR curve. There are three stages each of which corresponds to a specific physical phenomenon in the RSW process. Stage I indicates the intimate contact of workpieces and breakdown of asperities. With increased contact area, the DR unambiguously drops. Stage II is

Table 6 Confusion matrix for one attempt of training data in random forest classification (*ntree* = 1000, *mtry* = 4)

	Cold welds	Expulsion	Good welds	Classification error (%)
Cold welds	111	0	4	3.4
Expulsion	0	15	0	0
Good welds	9	1	108	8.5
Classification Rate			94.4%	

indicative of local melting and formation of the nugget. The bulk resistivity rises with ascending temperature. The elevated bulk resistivity outperforms the influence of contact area reduction in nugget nucleation, accounting for the rise of DR in stage II. After β peak, the DR curve gradually decreases with enlarged nugget diameter until reaching the end point in stage III.

In total, nine features (M = 9) were selected to describe the DR signature for the training dataset. These extracted features, shown in Fig. 5, include critical DR values of trough R_α, peak R_β, end point of DR curve R_γ, and their relative velocities for film breakdown v_1 (stage I), local melting and initiation of nugget formation v_2 (stage II), and nugget growth v_3 (stage III). The maximum absolute gradient in stage III ∇_{max} was also recorded to ensure the accuracy to distinguish minor expulsion from good welds. When minor expulsion takes place, the declines in DR sometimes may not differentiate from the good ones by only considering the overall gradient in stage III; the maximum absolute gradient can better describe the sudden change in DR. In addition, averaged DR value R and standard deviation σ of the DR curve were taken into account since the expulsion gives a rise on the precipitous drop in DR value.

Representative DR curves for three weld quality levels are plotted in Fig. 6, with an electrode force of 2.7 kN and a weld time of 12 cycles unchanged. Weld currents, ranging from 8 to 8.8 kA, resulted in cold welds, and weld current beyond 10.8 kA caused expulsion at the faying surface. Weld currents between 8.8 and 10.8 kA produced good welds. By combining the physical characteristics of DR curve, remarkable differences are observed from three quality levels. Cold welds do not obtain an apparent trough α and peak β, suggesting minor local melting and inadequate nugget formed. For good welds, their tendencies precisely resemble the typical DR curve of mild steel in RSW. Noticeably, the end point value of the good weld is substantially smaller than that of the cold weld. This trend shows that DR significantly drops during stage III owing to successive expanding nugget diameter. Two modes of expulsion were observed from the probed curves: early expulsion and late expulsion. It is evident that early expulsion is indicated by a remarkable drop in DR in Fig. 6 because the ejection of molten metals induces a substantial reduction in contact area. Late expulsion usually occurs in the last few half cycles of welding phase. The DR signature is quite different from that of early expulsion. However, the features extracted from the DR curves do not vary significantly.

Prior to training, the correlation analysis was adopted among extracted characteristics to evaluate if sufficient

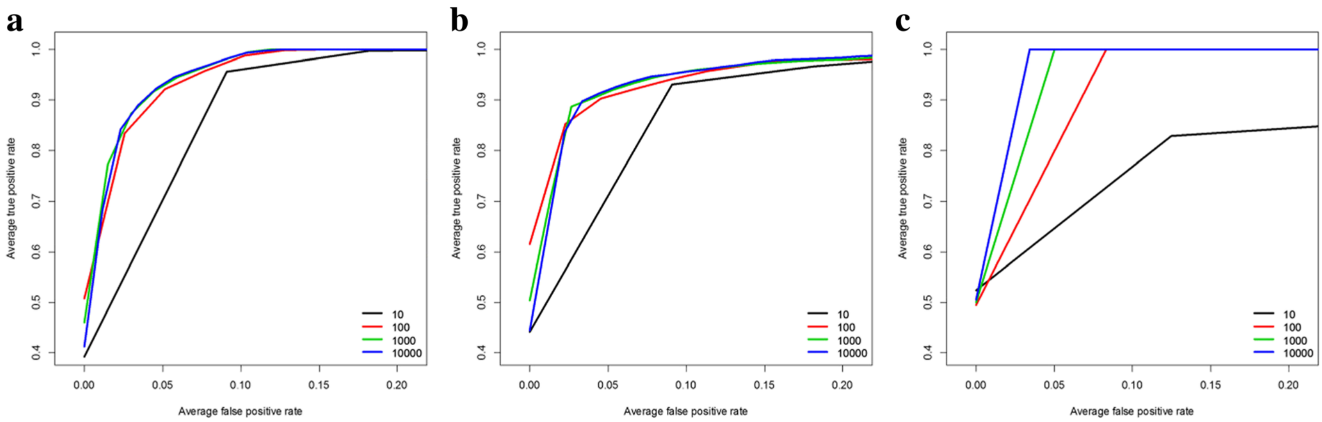

Fig. 8 Enlarged ROC curves based on influence of *ntree*. **a** IF. **b** PF. **c** Splash

parameters are extracted to establish a monitoring system. The correlation coefficient approaching to 1 or − 1 shows strong linearity between two variables; otherwise, the correlation coefficient approximating to 0 implies a weak relation to two variables. The correlation of 0.6 and above indicates a strong correlation. The inter-item correlation analysis among input variables is shown in Table 5. We identify that the R_α, R_β, and R have a strong correlation with each other and show very weak correlation with three gradients. R_γ and v_3, on the other hand, do have a strong relation with each other. In addition, three gradients for asperity collapse, nugget nucleation, and nugget growth do not have a significant correlation with each other. An increase in stage II does not necessarily infer a well-formed nugget. For cold welds, the values of v_3 are negligible. The overall gradient in stage III v_3 and maximum absolute gradient ∇_{max} share a strong correlation with each other, associated with the sudden decline of expulsion. The standard deviation σ shows a strong inverse correlation with the R_γ. This phenomenon can be understood by considering the DR response to expulsion. When expulsion occurs, a sudden drop in DR is noticed, which leads to a significant increase in σ.

3.3 Construction of RF classifier

RF method requires users to provide number of trees *ntree* and number of features to be used at each node *mtry* prior to the implementation. The choice of *ntree* and *mtry* substantially affects the accuracy of the model. Here, we firstly examined the parameter sensitivity of RF results. In this work, nine features (M = 9) were extracted from the DR signals, and the optimal value of *mtry* should approximate to $\sqrt{M}$ in classification [7]. We herein compare the *OOB* accuracy of RF models utilizing *mtry* that ranged from 1 to 6 and *ntree* from 10 to 10,000. By using the bootstrapping process, each tree was planted based on a different sample set from the training set. Test data, independent from the training set, were later utilized for prediction based on the constructed models.

The summary of the influence of *ntree* and *mtry* on *OOB* accuracy is presented in Fig. 7. It is clearly seen that the selections of *ntree* and *mtry* have a pronounced effect on *OOB* error. The accuracy of classification was

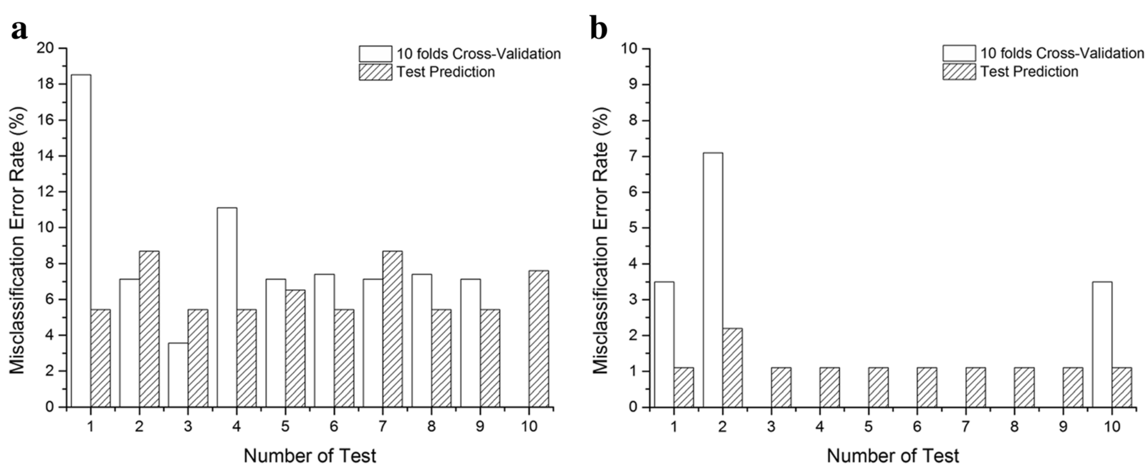

Fig. 9 Comparison of test error and CV error based on **a** DR signals, **b** DR, and weld parameters

Table 7 Variable importance of extracted features from DR curves

DR	Mean decrease in accuracy	DR and weld parameters	Mean decrease in accuracy
R_α	23.26	R_α	14.58
R_β	16.17	R_β	11.81
R_γ	50.18	R_γ	29.58
v_1	29.43	v_1	18.16
v_2	53.47	v_2	34.00
v_3	50.03	v_3	33.48
R	20.57	R	14.79
σ	21.41	σ	18.21
∇_{max}	58.42	∇_{max}	42.35
~	~	*WC*	77.26
~	~	*WT*	15.65
~	~	*EF*	9.23

strongly dependent on the amount of trees in the ensemble, and smallest *OOB* error was achieved by an ensemble of 10,000 trees. In contrast, ensembles of 10–100 trees tended to gain much higher *OOB* error rates. For the number of features considered at each node, *mtry* of 4 gave appealing performance over other selected values. By considering all circumstances, an RF with *ntree* = 1000 and *mtry* = 4 was constructed for the collected DR signals. A typical confusion table of the employed RF is presented in Table 6. The individual misclassification rates for cold welds, expulsion, and good welds were 3.4, 0, and 8.5%, respectively. Misclassification of good welds into cold welds accounts for the most of the errors made by the classifier. Based on the tensile-shear test, some joints have a failure load close to peak load of pull-out mode with low electrode force applied; however, it still fails in IF mode. Such samples cannot be well distinguished.

Columns stand for predicted class and rows stands for original judgments

Figure 8 shows average ROC curves of classifiers with varied *ntree* from 10 to 10,000, using the test dataset. Since ROC is specified for binary classification problem instead of multiclass classifier, we adopted "One-vs-All" approach to generate ROC curves [17]. Area under curve (AUC) of the multiclass classifier is calculated as

$$AUC = \frac{AUC_{IF} + AUC_{PF} + AUC_{Splash}}{3} \tag{3}$$

Higher value of *ntree* allows greater AUC in all three classes, where a greater AUC suggests a good classifier. AUCs for *ntree* of 10, 100, 1000, and 10,000 are 0.9890, 0.9926, 0.9931, and 0.9932, respectively. The increment in AUC from 10 to 100 trees outperforms the increments from 100 to 10,000 trees. Moreover, the AUCs of the PF classification are the lowest among the three classifiers, suggesting remained misclassification of PF into other classes.

The 10-fold cross-validation (CV) misclassification and test prediction error are compared in Fig. 9a. The averaged prediction error and the error induced from cross-validation were 6.4 and 7.6%, respectively. RF model based on DR profile quantity does not overfit. To further reduce the misclassification error between good welds and cold welds, three welding parameters (*WC*, *WT*, and *EF*) were added into the RF classifier. Ten independent sets of training and tests were carried out with RF parameter unchanged, as schemed in Fig. 9b. It is clear that both *CV* error and test error were significantly declined from the results relying on DR signals. Significant improvements in cross-validation error and prediction error are found. Averaged cross-validation error (1.4%) is slightly greater than test error (1.2%), indicative of no overfitting for the constructed models. The inclusion of weld parameters is proven to effectively optimize the classification rate.

4 Discussion

4.1 Variable importance evaluation

The variable importance of extracted DR features was investigated via permutation accuracy importance (PAI). The estimations of variable importance give a good implication on ranking the relative importance of input features in constructing the ensemble of decision trees. For k_{th} tree $h_i\{\boldsymbol{X}\}$ (i = 1,2… k) built in the forest, it corresponds to a unique bootstrapping data and out-of-bag data. The classification is employed based on the *OOB* data, and the count of the accurate classification R_b^{OOB} is estimated accordingly. For a *ntree* model, the out-of-bag error rate is determined. Then, feature m_i (i = 1,2…M) used in the data set is randomly permutated once per time and the procedure in building RF and estimating *OOB* error is repeated based on newly permutated variables. The importance measure D_j for variable m_i and z-score are given by the following:

$$D_j = \frac{1}{M}\left(R_b^{OOB} - R_{bj}^{OOB}\right) \tag{4}$$

$$z_j = \frac{D_j}{s_j\sqrt{M}} \tag{5}$$

s_j is the standard derivation of the decrease in classification on undistorted data. Then, z_j is transformed into a significance value based on the assumption of Gaussian distribution.

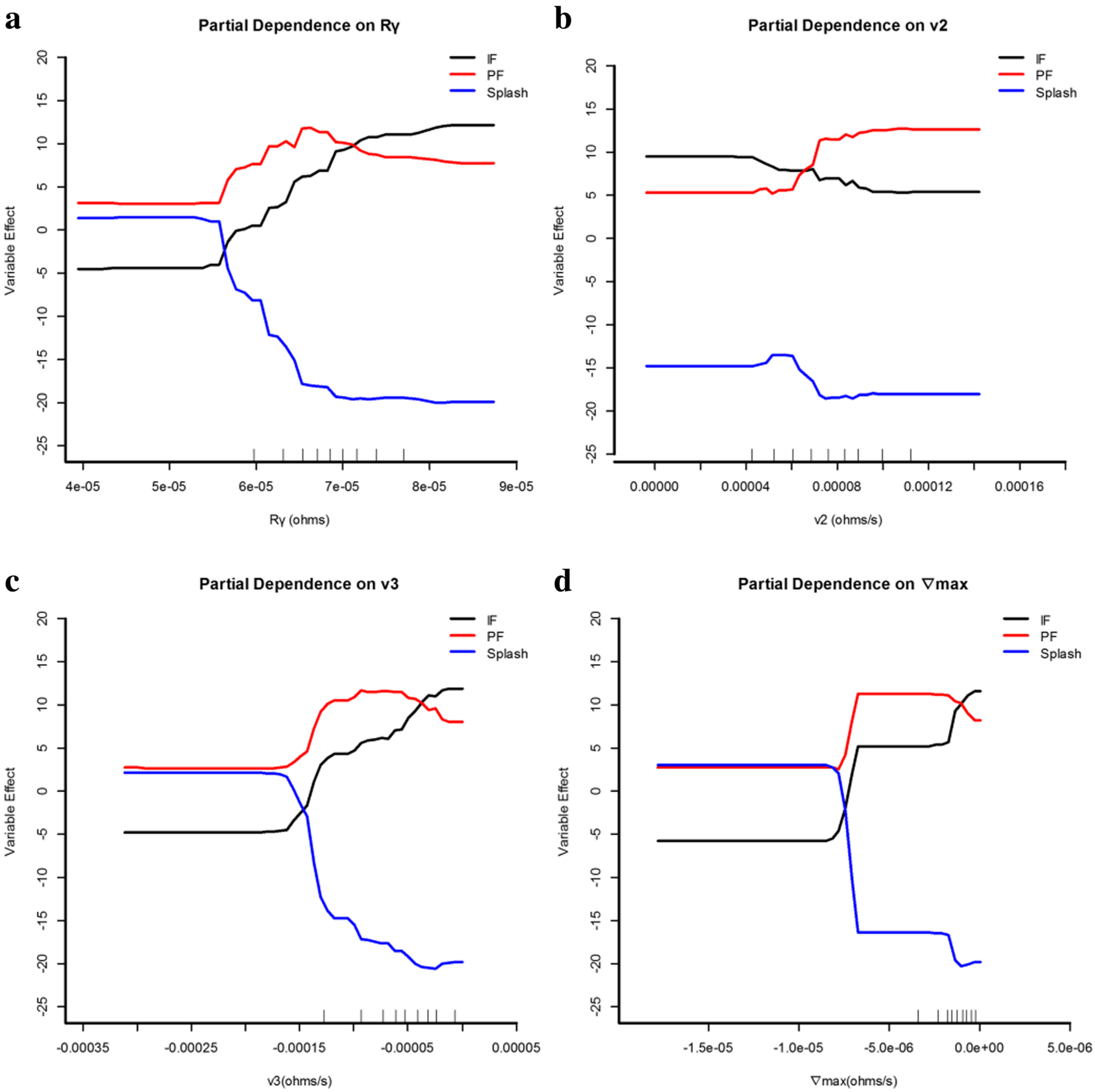

Fig. 10 Partial dependence plots of significant features. **a** R_γ. **b** v_2. **c** v_3. **d** ∇_{max}

We here conducted variable importance evaluation on two optimum RF systems in the previous section. Mean decrease in accuracy stands for significance of the variables after permutation of the values. In Table 7, it is clearly spotted that four features R_γ, v_2, v_3, and ∇_{max} extracted from DR have the most significant impact on decision-making for the DR-based RF classifier. Other five parameters are less important based on the mean decrease in accuracy value. Recall from the inter-item correlation analysis, v_3 and ∇_{max} have a strong inter-correlation. Hence, both of them are found to play crucial roles in classifying weld quality. It is intriguing that independent slopes v_2 and v_3 are influential for RF classifier accuracy. When sufficiently large current flows through the workpieces, asperity collapse occurs which increases the contact area. Large gradient of v_2 infers that the heat input results in substantial film breakdown and enlarged contact region and local melting at the faying surface. Moreover, a descending trend (significant v_3 and $\nabla_{\max}$ and small R_γ) in DR during nugget

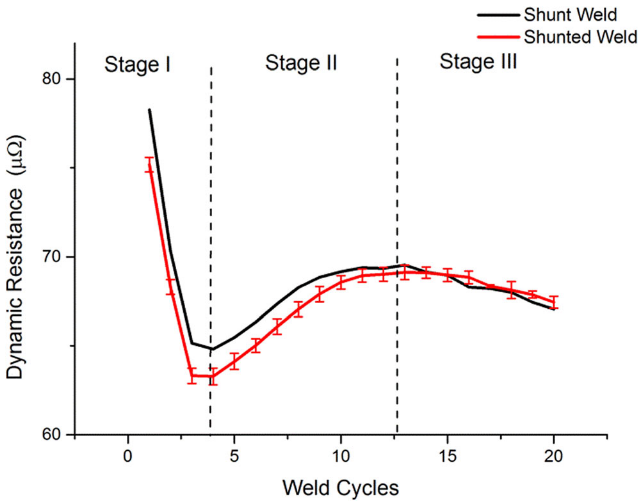

Fig. 11 Shunting effect in DR curves (weld spacing equals 20 mm)

growth indicates an inverse relationship with the final nugget diameter. Expulsion accounts for the precipitous decline in DR and contributes to a much smaller R_γ compared to those of good welds. Factors like R_α, R_β, and v_1 are more closely related to the initial surface condition and contact status of the faying surface than the nugget growth in stages II and III are.

In Luo's work, it is straightforward to adopt the relative averaging value of DR to distinguish weld quality [5]. Unlike the existing approach in differentiating the weld quality, good welds and poor welds have little difference in the average values R and standard derivation σ in DR curves. It might result from different approaches to calculate the DR values. Similarly, Wan adopted principal component analysis (PCA) on discrete points on the DR curves [11]. Five principal components were selected over PCA, accounted for over 99.6% proportion, and the first component (PC1) attained accountability proportion of 78.3%. However, we fail to interpret the actual physical meaning of the principal components extracted from the curve. When inadequate sized welds occur in the production line, indication from the derived principal components is limited. On the other hand, R_γ, v_2, v_3, and ∇_{max}, the most significant variables of RF, allow user to examine the actual history of nugget development and take actions to avoid succeeding undersized welds. Moreover, to adopt PCA with varied welding time, users need to ensure the same dimensionality for the original data. The generated result may hardly differentiate the significance of welding time, which needs to be corrected by inputting actual weld time into the model.

Table 8 Confusion matrix for DR curves without shunted welds in random forest classification (*ntree* = 1000, *mtry* = 4)

	Cold welds	Expulsion	Good welds	Classification error (%)
Cold welds	83	0	7	7.7
Expulsion	0	21	1	4.5
Good welds	8	1	106	7.8
Classification Rate			92.6%	

For DR and weld parameter-based RF classifier, the choice of *WC* becomes the most important value in determining the classification accuracy, over four features R_γ, v_2, v_3, and $\nabla_{\max.}$ *WT* and *EF* are considered as less important features for the classification, owing to the relatively narrow range compared to weld current and minor contribution based on the Joule's equation.

We further investigated the partial dependence of significant features on the classification probability. We used R language "partial plot" function to calculate the partial dependence [16].

$$\tilde{f}(x) = \frac{1}{n}\sum_{i=1}^{n} f(x, x_{ic}) \tag{6}$$

$$f(x) = logp_k(x) - \frac{1}{K}\sum_{j=1}^{K} logp_j(x) \tag{7}$$

where x is the variable of interest and x_{ic} is the rest of variables in the data, K is the number of classes, k is the class to be investigated, and p_j presents the fraction of the vote for j. A positive value in $\tilde{f}(x\ )$ increases the probability of the corresponding class, and vice versa. Here, we present partial dependence of previously discussed features on three weld classes in Fig. 10. For R_γ, v_3, and ∇_{max}, they attain nearly identical plots though corresponding x values are different. To single out splash from other weld types, the feature values need to be smaller than a threshold value, which are 5.5e-05 Ω, 1.8e-04 Ω/s, and 0.75e-05 Ω/s, respectively. Moreover, classification of IF and PF mode is accomplished by the intersection point in each sub-plot. When greater variable effect of PF mode is located between 5.5 e-05 and 7.2 e-05 Ω, R_γ is more likely to predict the weld quality as PF mode. On the other hand, v_2 displays opposite trend in distinguishing IF and PF mode, while impact of the variable on expulsion keeps negative. It suggests that v_2 has negligible connection with the phenomenon of expulsion and fails to solely predict expulsion since it accounts for nugget growth velocity in stage II.

4.2 Shunting effect in DR curves

In this work, there are two ways to produce RSW joints: making consecutive welds on the same sheet

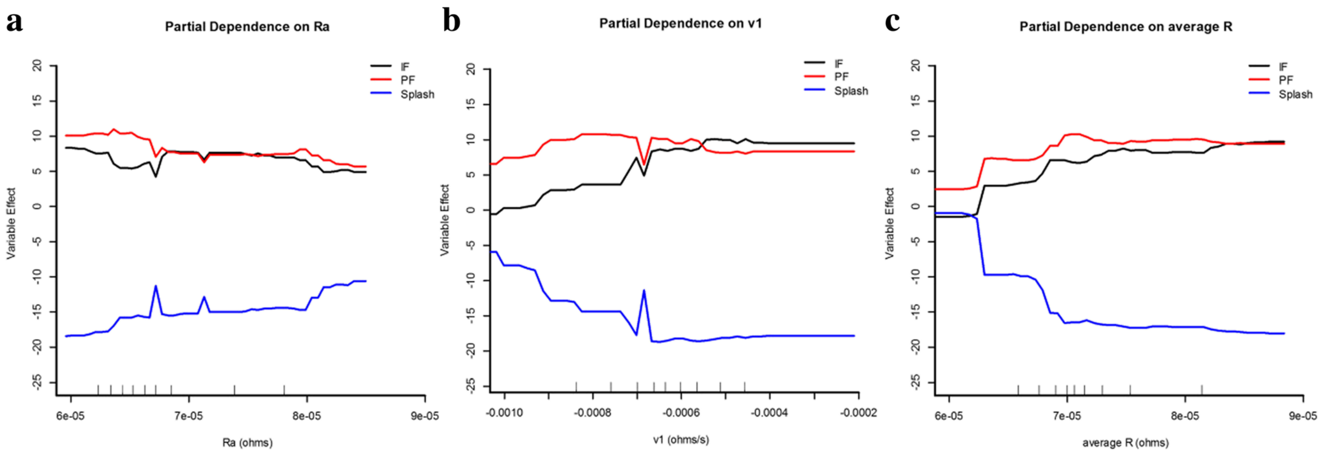

Fig. 12 Partial dependence plots of significant features. **a** R_α. **b** v_1. **c** R.

and making new welds on every new sheet. The former joints resemble the production sequence in the plant environment. The latter joints, on the other hand, are prepared into the tensile shear specimen and provide an indication of weld quality at that welding schedule. However, consecutive welds on the same sheet give a rise on shunting effect. Though identical welding parameters were applied to the group of welds, the differentiation in contact status between the faying surface and workpiece/electrode surface and shunting current may result in different DR curves. Shunting current effect is considered as the predominant influence for the qualities of consecutive welds and resulted quality control system, where the resulted DR of continuous welds (shunted weld) may be smaller than the first weld on the workpiece (shunt weld), according to the equation:

$$R_{DR} = \frac{R_w \times R_s}{R_w + R_s} \tag{7}$$

where R_{DR} is the resulted DR derived by measured voltage and current, R_w is the effective resistance of the weld path, and R_s is the effective resistance of the shunting path, which is proportional to the weld spacing. Though, in this study, the weld spacing is equal to the minimum distance for mild steel (20 mm) [13]. DR curves of the shunt and shunted welds are compared in Fig. 11. It is clearly seen that the difference in DR value is significant at stage I between shunt and shunted welds and the gaps become narrower in stages II and III. In addition, based on eq. (7), it is inevitable that the values of R for shunted welds are smaller than those of shunt welds.

To investigate the influence of shunting, another DR-based RF classifier was constructed (*ntree* = 1000, *mtry* = 4), with all shunted weld excluded from the original data source. In total, 228 samples were used. The resulted confusion matrix schemed in Table 8, however, does not show any significant improvement in classification accuracy (about 92.6%). From partial dependence shown in Fig. 12, the variations in R_α and v_1 and R do not substantially affect the probability of classification among the varying range. Hence, the improvement in accuracy is negligible after excluding all shunted welds. In this case, the consecutive welds with weld spacing beyond minimum values (20 mm for mild steel) do not significantly affect the classification accuracy. Wen's work revealed the inverse relationship of nugget diameter and endpoint value of DR curves of stainless steel and the DR curves of weak and severe shunting [18]. Shunting proportionally decreases endpoint value of DR values with weld spacing, making it inconsistent with previous relationship found with nugget diameter. Thus, this finding gives an implication that RF classifier may have difficulties in distinguishing undersized welds due to severe shunting in consecutive welds if no more information is provided.

Columns stand for predicted class and rows stand for original judgments

5 Conclusion

RF classifier was adopted on dynamic resistance in RSW. Three levels of weld quality were considered as classes in this study, with regards of cold weld, good weld, and expulsion. The values of *ntree* and *mtry* substantially affect the performance of the classifier, which is revealed via *OOB* error and AUC. The preliminary results showed that RF can give a satisfying classification (~ 93.6%) based on the DR profile quantities. The introduction of weld parameters into classifier substantially improves predicted classification accuracy (98.8%). Using variable importance evaluation by RF, four DR profile features and weld current are considered as the most important variables for the classifiers, which is not available from other black-box models. However, v_2 provides little information in classifying expulsion as rest of features. Issues were also identified for the RF classifier. The misclassification in good welds into cold weld was predominant, which still requires human operator interpretation. Shunted welds with sufficient weld spacing do not significantly undermine the accuracy for RF classifier. Further works on severe shunting are expected to be performed. By incorporating RF classifier, the online quality monitoring system is proposed to evaluate every weld made on the production line.

Acknowledgements The financial support from the Australian Research Council (Grant No. LP130101001) is fully acknowledged. The authors would like to thank Dr. David Adam and Mr. Cameron Summerville from The Australian National University for assistance with experiment set-up.

Compliance with ethical standards

Funding This study was funded by Australian Research Council (Grant No. LP130101001).

Conflict of interests The authors declare that they have no competing interests.

References

1. Zhang H (1999) Expulsion and its influence on weld quality. *WELD J-NEW YORK* 78:373-s
2. Liu J, Xu G, Gu X, Zhou G (2015) Ultrasonic test of resistance spot welds based on wavelet package analysis. Ultrasonics 56:557–565
3. Wang H, Zhang Y, Chen G (2009) Resistance spot welding processing monitoring based on electrode displacement curve using moving range chart. Measurement 42:1032–1038
4. Gedeon S, Sorensen C, Ulrich K, Eagar T (1987) Measurement of dynamic electrical and mechanical properties of resistance spot welds. Weld J 66:378–385
5. Luo Y, Rui W, Xie X, Zhu Y (2016) Study on the nugget growth in single-phase AC resistance spot welding based on the calculation of dynamic resistance. J Mater Process Technol 229:492–500
6. Fan Q, Xu G, Gu X (2016) Expulsion characterization of stainless steel resistance spot welding based on dynamic resistance signal. J Mater Process Technol 236:235–240
7. Breiman L (2001) Random forests. Mach Learn 45:5–32
8. Martín Ó, Pereda M, Santos JI, Galán JM (2014) Assessment of resistance spot welding quality based on ultrasonic testing and tree-based techniques. J Mater Process Technol 214:2478–2487
9. Pereda M, Santos J, Martín Ó, Galán J (2015) Direct quality prediction in resistance spot welding process: sensitivity, specificity and predictive accuracy comparative analysis. Sci Technol Weld Join 20:679–685
10. Zhang P, Zhang H, Chen J, Ma Y (2007) Quality monitoring of resistance spot welding based on electrode displacement characteristics analysis. Front Mech Eng China 2:330–335
11. Wan X, Wang Y, Zhao D (2016) Quality monitoring based on dynamic resistance and principal component analysis in small scale resistance spot welding process. Int J Adv Manuf Tech 86(9–12): 3443–3451
12. Zhang H, Wang F, Xi T, Zhao J, Wang L, Gao W (2015) A novel quality evaluation method for resistance spot welding based on the electrode displacement signal and the Chernoff faces technique. Mech Syst Signal Process 62:431–443
13. Wang B, Lou M, Shen Q, Li Y, Zhang H (2013) Shunting effect in resistance spot welding steels—part 1: experimental study. Weld J 92:182–189
14. AWS D17.2 (2007) Specification for Resistance Welding for Aerospace Applications
15. Long H, Hu Y, Jin X, Shao J, Zhu H (2016) Effect of holding time on microstructure and mechanical properties of resistance spot welds between low carbon steel and advanced high strength steel. Comput Mater Sci 117:556–563
16. Liaw A, Wiener M (2002) Classification and regression by randomForest. R news 2:18–22
17. Provost F, Domingos P (2000) Well-trained PETs: improving probability estimation trees. CeDER Working Paper #IS-00-04, Stern School of Business, New York University, NY 10012
18. Wen J, Wang C, Xu G, Zhang X (2009) Real time monitoring weld quality of resistance spot welding for stainless steel. ISIJ Int 49: 553–556